Ann. Solid Struct. Mech. (2013) 5:15–34
DOI 10.1007/s12356-013-0033-8

ORIGINAL ARTICLE

A 3D nonlinear static analysis of long-span cable stayed bridges

D. Bruno · F. Greco · P. Nevone Blasi · E. Bianchi

Received: 7 December 2012 / Accepted: 19 June 2013 / Published online: 4 July 2013

Abstract A numerical investigation on the nonlinear static behavior of self-anchored long span cable-stayed bridges with a fan-shaped arrangement of stays is carried out by adopting a spatial finite element model of the bridge. An equivalent continuous model of the bridge is also developed in order to point out the main parameters governing the non-linear behavior of the bridge to be used in the more general 3D discrete bridge analysis and to provide a validation of the discrete model. The importance of an accurate description of geometrically nonlinear effects arising from the stays nonlinear response in coupling with the instability effect of axial compression in girder and pylons, is evaluated by means of original comparisons with results obtained by using simplified assumptions. Novel parametric studies are performed for investigating the influence of the main geometrical and material design parameters derived from the continuous model formulation on the maximum load-carrying capacity of the bridge and related collapse mechanisms. Different loading conditions, also including live load eccentricities, and pylon shapes are also considered and a nonlinear procedure for finding the initial geometry and prestress distribution under dead load is incorporated in the analysis. The results point out the strong role of nonlinear stays response, especially when the assumed loading condition produces cable unloading, in coupling with the notable influence of the relative girder stiffness on the stability bridge behavior. On the contrary, in general pylon shape and stiffness, live load eccentricity and torsional stiffness are less important factors in nonlinear analysis.

Keywords Geometrical nonlinearities · Nonlinear stay behavior · Numerical finite element model · Stability · Cable-stayed bridge

List of symbols

a	Sag effect and stays deformability parameter
A_0	Anchor stay cross sectional area
A_s	Stay cross sectional area
b	Cross-section half width of the girder
C_t	Girder torsional stiffness
E	Young modulus
e	Load eccentricity
EA	Girder axial stiffness
EI	In-plane girder flexural stiffness
$EI_{p\ xx}$	Out-of-plane tower bending stiffness
$EI_{p\ yy}$	In-plane tower bending stiffness
EI_{zz}	Out-of-plane girder bending stiffness
E_s^*	Dischinger's secant modulus of the stay
E_t^*	Dischinger's tangent modulus of the stay
g	Dead load
I_r	Tower to girder in-plane bending stiffness ratio
K	Pylon top flexural stiffness
K_u	Fictitious beam axial stiffness
K_ψ	Fictitious beam torsional stiffness
L	Central span length of the bridge
l	Lateral span length of the bridge
L_e	Element length
l_o	Horizontal projection of the stay length
m_f	Horizontal flexural couple of the stays-girder interaction

D. Bruno (✉) · F. Greco · P. Nevone Blasi · E. Bianchi
Department of Structural Engineering, University of Calabria, Cosenza, Italy
e-mail: d.bruno@unical.it

mt	Torsional couple of the stays-girder interaction
N^g	Axial force in the girder due to the dead load g
$N_1^0, \ldots, N_n^0$	Pretension forces in the double curtain of stays
p	Live load
q_h	Horizontal component of the stays-girder interaction
q_v	Vertical component of the stays-girder interaction
S_0	Horizontal component of the anchor stays axial force
u	Pylon tops horizontal displacement
$\bar{u}^{(l)}, \bar{v}^{(l)}, \bar{w}^{(l)}$	Prescribed displacements on left anchor point
$\bar{u}^{(r)}, \bar{v}^{(r)}, \bar{w}^{(r)}$	Prescribed displacements on right anchor point
$v(z)$	Girder vertical displacements
$w(z)$	Girder horizontal displacement
γ	Cable weight per unit volume
ε	Relative in-plane bending stiffness of the girder
ε_A	Relative axial stiffness of the girder
θ_x	Bending rotation about the x axis in the discrete model
θ_y	Bending rotation about the y axis in the discrete model
θ_z	Bending rotation about the z axis in the discrete model
σ_0	Initial stress in the stay
τ	Relative torsional stiffness of the girder
$\Delta N(w)$	Axial force increment in the girder due to live loads
$\Delta\varepsilon$	Strain increment in the stay
$\Delta\sigma$	Stress increment in the stay
Δ	Stays spacing
δ_l	Lateral midspan deflection
$\delta\boldsymbol{u}$	Incremental kinematically admissible displacements
ε_h	Relative out-of-plane bending stiffness of the girder
λ_c	Critical load
λ_{max}	Maximum load
λ	Load parameter
Π	Total potential energy functional
$\theta(z)$	Girder torsional rotation
σ_a	Allowable stress for the stays
σ_g	Stay tension under dead load g
σ_{g0}	Anchor stay tension under dead load g
ψ	Pylon tops torsional rotation

1 Introduction

Due to the notable progress in structural engineering, material and construction technologies, cable-stayed bridges have become an efficient solution for long span crossing [1–4]. As a matter of fact in this kind of construction, consisting of three main components (namely girders, towers and inclined cable stays), the girder, supported elastically by inclined cable stays, can span a much longer distance without intermediate supports. On the other hand, the dead load and live load on the girder are transmitted to the towers by inclined cables exhibiting high tensile forces which in turn induce high compression forces in towers and girder.

Long span cable-stayed bridges exhibit a remarkable nonlinear behavior under dead and live loads. Nonlinear effects in cable stayed bridges may arise from different sources, including the nonlinear behavior of a single stay exhibiting a different response in loading and in unloading due to the cable sag effect induced by dead load, changes in geometrical configurations due to large deflections effects (usually large rotations but small strains) in both towers and girder due to their slenderness, the geometrical instabilizing effect of the axial compression induced in the towers and girder by inclined stays, as well as the interactions between cables, deck and pylons nonlinearities [5–7]. Other nonlinear effects may be related to the constitutive behavior of materials [8–10] or to the coupling between torsion and bending of the girder.

Considerable attention has been devoted in the literature to the nonlinear structural behavior problem of cable-stayed bridges [5–17]. In order to reduce the complexity of the highly non-linear problem, most studies available in the literature have introduced some reasonable assumptions in their formulations including one or more of sources of nonlinearities.

For instance, pylons nonlinearities arising from beam-column effect are often neglected assuming a high flexural stiffness in pylons [12]. An in-plane analysis is typically carried out excluding out-of-plane and torsional deformation modes and their interaction [5, 6, 9, 11, 12, 15], which can be usually not important in absence of eccentric loading also when a three-dimensional bridge model is developed [7, 13]. The prebuckling behavior is often assumed to evolve linearly with the load parameter, such that prebuckling displacements, stresses and strains vary linearly with the load parameter thus leading to a linear eigenvalue problem for the critical load [7, 11, 16]. The cable is frequently considered as a straight truss element for the whole inclined cable stay with uniform properties from end to end incorporating the sag effect by means of

the equivalent modulus of elasticity corresponding to the tangent Dischinger's fictitious modulus under the hypothesis that the change in tension in the cable during a load increment is not large [8, 17]. Moreover, often the truss element is assumed to have a tension-only behavior, namely in order to take into account for stiffness reduction in compression the tangent modulus is assumed to vanish when shortening occurs [5, 6, 14, 16]. In addition, the initial configuration of the bridge under dead loads has been determined adopting several methods, ranging from nonlinear optimization procedures to simplified techniques for estimating initial cable forces based on equilibrium requirements [5, 6, 9, 12, 18, 19].

Although most nonlinear analyses have focused on geometrical nonlinear effects some analyses have involved both geometric and material nonlinearities and analyzed the ultimate behavior and load capacity of a cable-stayed bridge [8–10, 17, 20].

Due to its inherently nonlinear behavior a conventional analysis of the cable-stayed bridge, based on linear assumptions and on the tangent value of the equivalent elasticity modulus [15, 21], is often not applicable especially for long span bridges for which the main girder has the tendency to become more slender and lighter [12, 13, 22]. Existing models which do not take into account appropriately for the softening cable behavior under unloading related to cable sag geometrical nonlinearities, such as those based on the equivalent tangent modulus of elasticity or those assuming that the cable resists only tensile axial force with no stiffness against axial compression (tension only truss behavior) may lead to a notable underestimation of the maximum load carrying capacity of the bridge for specific loading conditions. Moreover, since axial compression in girder and pylons increases with the length of the central span, the stability of these members becomes an important aspect in the design of cable-stayed bridges [7, 11]. However, the actual prebuckling behavior of the bridge may deviate notably from the linear assumptions depending on the specific loading condition and a nonlinear limit point analysis should be carried out in place of a linear stability analysis [9].

As a consequence, a more realistic nonlinear structural analysis taking into account for a precise evaluation of the most important geometrically nonlinear effects should be adopted in conjunction with a nonlinear stability one. To this aim this contribution proposes a numerical investigation on the nonlinear static behavior of long span cable-stayed bridges with a fan-shaped arrangement of stays, by considering the nonlinear behavior of the single stay in coupling with the instability effect of the axial compression in both girder and pylons. In the sake of simplicity material nonlinearities have not been considered here.

After an introductory analysis illustrating the general features of the buckling and post-buckling behavior of the cable stayed bridge together with its stability behavior by using also a discrete example, the analysis is carried out numerically by introducing a general nonlinear cable stayed bridge model. Firstly a simplified continuous model, assuming a continuous distribution of the stay stiffness along the girder, is briefly introduced in order to determine the main parameters governing the non-linear behavior of the bridge in view of the subsequent parametric analysis based on the more general 3D discrete bridge model. The resulting nonlinear differential problem is also numerically integrated with reference to an in-plane analysis case and thus obtaining results able to capture the main non-linear effects on the static response. Therefore a nonlinear three-dimensional finite element model of the bridge is formulated to accurately determine the influence of nonlinear effects on the nonlinear structural bridge behavior and on its maximum load carrying capacity. The cable system is modeled according to the multi element cable system approach, where each cable is discretized using multiple truss element and large deformations are accounted by using Green–Lagrange strains. The bridge has been modeled by means of a 3D assembly of non-linear beam elements and the connections between cables and girder have been obtained by using constraint equations. Comparisons between predictions obtained by using the continuous and the discrete models are carried out in order to check the limit of validity of the continuous formulation and to assess the accuracy of the subsequent parametric analyses based on continuous model results.

The significance of geometrically nonlinear effects on the bridge structural analysis is investigated by means of original comparisons with results obtained by using simplified assumptions regarding nonlinear stays behavior, namely the tangent modulus approximation and the tension-only model. This aspect, scarcely analyzed in previous studies to the authors' knowledge, is here investigated in a general context by including an accurate modeling of the different sources of geometrical-nonlinearities arising from cable sag effects and instabilizing effects of axial compression in both girder and pylons. Novel parametric studies are performed with reference to the 3D FE model for investigating the importance of the main geometrical and material design parameters on the nonlinear structural behavior of the bridge in presence of both in-plane and out-of-plane deformation mechanisms. Different loading conditions, also including live load eccentricities, and pylon shapes are also considered and a nonlinear procedure for finding the bridge initial shape is incorporated in the analysis in order to determine properly the initial geometry and prestress distribution under

dead load. This represents another aspect of novelty of the paper since in previous parametric studies existing in the literature various simplified assumptions have been introduced including one or more sources of nonlinearities.

2 Preliminary remarks and overview of nonlinear bridge behavior

2.1 Nonlinear cable behavior

Cable response is one of the most relevant sources of nonlinear behavior of cable-stayed bridges and, as a consequence, it must be accurately considered in cable-stayed bridge design in order to avoid inappropriate predictions of the actual load carrying capacity.

As far as the assumptions regarding stay response are concerned it must be evidenced that the for large stress increments the secant modulus of the stress–strain relationship must be adopted instead of the tangent one, due to the high geometrical nonlinearity related to dead load of the stay.

The stress increment $\Delta\sigma$ in the stay may be written in the form:

$$\Delta\sigma = E_s^*(\Delta\varepsilon)\Delta\varepsilon, \tag{1}$$

where E_s^* is the secant modulus of the stay depending nonlinearly on the axial strain $\Delta\varepsilon$ (see Fig. 1). It is worth noting that the axial strain is measured along the stay chord (dashed line in Fig. 1).

Assuming a parabolic approximation of the stay deformed configuration, the secant modulus has the following expression showing the nonlinear dependence on the stress increment and the different behavior under positive or negative strain increments (see [1]):

$$E_s^* = \frac{E}{1+\frac{\gamma^2 l_0^2 E}{12\sigma_0^3}\frac{1+\beta}{2\beta^2}}, \quad \beta = 1+\frac{\Delta\sigma}{\sigma_0}, \tag{2}$$

where E is the Young modulus, A the cable cross-sectional area, γ the cable weight per unit volume, l_o the horizontal projection of the stay length, and σ_0 the initial stress in the stay. On the other hand, for small stress increments from the initial configuration (i.e. $\beta \to 1$), the cable equivalent modulus of elasticity can be considered constant during load increment and the nonlinear cable response can be approximated by means of the tangent modulus given by the well-known Dischinger's formula (see [1, 15, 21]):

$$\frac{\Delta\sigma}{\Delta\varepsilon} = E_t^* = \lim_{\beta\to 1} E_s^* = \frac{E}{1+\frac{\gamma^2 l_0^2 E}{12\sigma_0^3}}. \tag{3}$$

Assuming that when shortening occurs the cable stiffness vanishes leads to the tension only approximation of stay behavior (see for instance [5, 6, 14, 16]):

$$\frac{\Delta\sigma}{\Delta\varepsilon} = \begin{cases} E_t^* & \text{if } \Delta\varepsilon \geq 0 \\ 0 & \text{if } \Delta\varepsilon \leq 0 \end{cases}. \tag{4}$$

when the cable sag effect is neglected E_s^* can be replaced by E.

In order to analyze the nonlinear stay response it is convenient to obtain an asymptotic expansion of the secant modulus Eq. (2) as a function of the axial strain:

$$E_s^*(\Delta\varepsilon) = E_0^* + E_1^*\Delta\varepsilon + E_2^*\Delta\varepsilon^2 + O(\Delta\varepsilon^3). \tag{5}$$

The remaining terms can be obtained by considering the Taylor series expansion of Eq. (2) up to the second order as a function of $\Delta\sigma$:

$$E_s^*(\Delta\sigma) = E_t^* + \frac{3aE}{2(1+a)^2\sigma_0}\Delta\sigma + \left(\frac{9a^2E}{4(1+a)^3\sigma_0^2} - \frac{2aE}{(1+a)^2\sigma_0^2}\right)\Delta\sigma^2 + O(\Delta\sigma^3), \tag{6}$$

and by substituting $\Delta\sigma$ as a series expansion of $\Delta\varepsilon$ up to the second order by using Eqs. (1) and (5):

$$\Delta\sigma = E_0^*\Delta\varepsilon + E_1^*\Delta\varepsilon^2 + O(\Delta\varepsilon^3).$$

By comparing the terms of the same power in Eqs. (6) and (5) we obtain that the term of order zero E_0^* can be identified with the tangent modulus E_t^*, whereas the first and second order terms E_1^* and E_2^* are respectively:

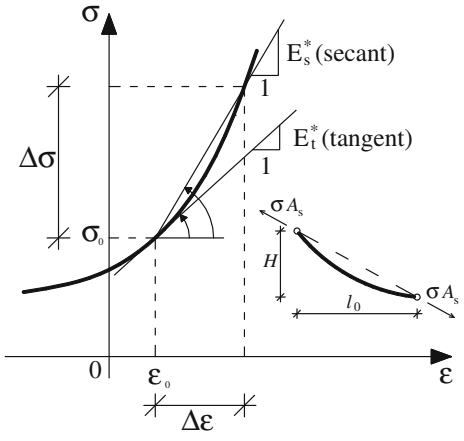

Fig. 1 Axial stress–strain constitutive cable behavior

$$E_1^*/E_t^* = \frac{3aE}{2(1+a)^2\sigma_0}, \quad E_2^*/E_t^* = \frac{(5a-4)aE^2}{2(1+a)^4\sigma_0^2},$$
$$a = \frac{\gamma^2 l_0^2 E}{12\sigma_0^3}. \tag{7}$$

It is worth noting that the parameter a accounting for the sag effect and defining stays deformability usually assumes values lower than unity (0.1–0.2) and consequently E_1^* is positive whereas E_2^* assumes negative values.

The effects of the above assumptions on the nonlinear cable behavior, can be analyzed qualitatively by considering a complete fan shaped and self-anchored scheme with the girder not constrained in the horizontal direction and the load uniformly applied on the central span. Generally speaking assuming a linear prebuckling behavior the girder's compression produces an equilibrium bifurcation when the load reaches the critical value. The postbuckling behavior strictly depends on the shape of the buckling mode and may show a decreasing behavior due to the softening cable response in compression (see the dashed line curve in Fig. 2).

The actual bridge behavior taking into account the nonlinear prebuckling effects, doesn't exhibit an equilibrium bifurcation and is qualitatively shown by means of a continuous line in Fig. 2, where it can be noted that the actual bridge behavior is similar to that of a structure with initial imperfections whose initial postbuckling behavior is determined by that of the idealized perfect structure. Generally speaking a snap buckling behavior is expected with a local maximum in the static equilibrium path at a value less than the critical load. The magnitude of the load maximum can be significantly below of the critical load as in imperfection sensitive structures. This behavior is mainly attributed to the softening behavior of the stress–strain stay relationship under shortening.

As a matter of fact, when the secant modulus model is adopted a strong snap buckling behavior is expected with a load maximum λ_{max} significantly below the critical load λ_c and post-buckling behavior of asymmetric unstable type being related to the higher order terms in the expansion of E_s^* shown in Eq. (5). On the other hand, when the cable behavior is modeled by means of the tangent modulus an unconservative prediction can be obtained since the limit load is larger than the more accurate one based on the secant modulus formulation and a mild snap buckling occurs as in a symmetric unstable bifurcation. The magnitude of the critical load, depending exclusively on the tangent modulus distribution along the stays, changes slightly with respect to the secant modulus

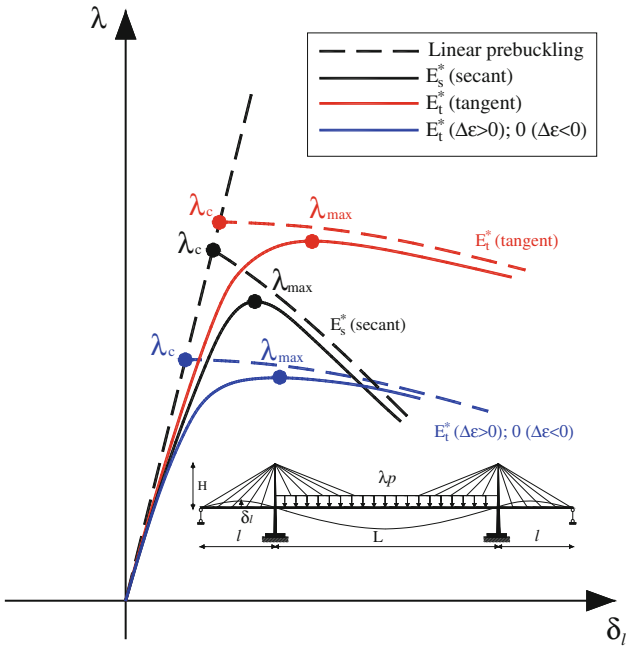

Fig. 2 Nonlinear bridge behavior in terms of load parameter versus lateral midspan deflection curve

formulation. For instance, the critical load should remain unchanged provided that for each stay the stress at bifurcation is adopted as initial stress in the tangent modulus formula. Note that when buckling occurs at higher load levels, as in the case of uniform loading on the entire bridge, a value near to E can be assumed for the tangent modulus.

A similar behavior occurs when the tension only truss model is adopted but the maximum load may be notably lower than the more accurate prediction obtained using the secant modulus model, thus leading to a conservative prediction of the maximum load-carrying capacity.

The above preliminary study of the bifurcation buckling is not complete without some attention to stability considerations. According to the incremental static stability criterion, the examined equilibrium configuration C is considered stable if the second order approximation of the difference between the internal deformation work and the external work of distributed dead loading λq during an incremental deformations from C to an adjacent configuration C′ is positive for all incremental kinematically admissible (*K.A.*) deformations $\delta \boldsymbol{u}$. This criterion coincides with the condition of a local minimum of the total potential energy functional and restricting the attention to an in-plane stability analysis, for the sake of simplicity, the stability functional for the bridge model shown in Fig. 3, assumes the following expression:

$$\begin{aligned}\Delta\Pi &= \Pi(\boldsymbol{u}+\delta\boldsymbol{u}) - \Pi(\boldsymbol{u}) \\ &\cong \frac{1}{2}\int_{-l-L/2}^{l+L/2} \left(EI\delta v''^2 + EA\delta w'^2 + N(\boldsymbol{u})\delta v'^2\right)dz \\ &+ \sum_{L+R}\frac{1}{2}\int_{0}^{h+H}\left(EI_P\delta v''^2 + EA_P\delta w'^2 + N(\boldsymbol{u})\delta v'^2\right)dz_P \\ &+ \frac{1}{2}\sum_{i=1}^{n_L}\frac{E_t^*(\boldsymbol{u})A_{Si}H}{\sin\alpha}\delta\varepsilon_L^2 + \frac{1}{2}\sum_{i=1}^{n_R}\frac{E_t^*(\boldsymbol{u})A_{Si}H}{\sin\alpha}\delta\varepsilon_R^2 \\ &+ \frac{1}{2}\frac{E_{t0L}^*(\boldsymbol{u})A_{0L}H}{\sin\alpha_0}\delta\varepsilon_{0L}^2 \\ &+ \frac{1}{2}\frac{E_{t0R}^*(\boldsymbol{u})A_{0R}H}{\sin\alpha_0}\delta\varepsilon_{0R}^2 > 0 \quad \forall\delta\boldsymbol{u}\neq\boldsymbol{0} \quad K.A. \end{aligned} \tag{8}$$

where according to the linearized theory of elastic stability (see [23, 24] for instance), taking into account that the current equilibrium configuration C is close to the initial one C_o the stability functional is evaluated directly on the initial configuration C_o, namely the incremental elastic response of bridge components (girder, pylons and stays) is evaluated in the natural configuration and the axial stress distribution in the girder $N(\boldsymbol{u})$ due to dead loading in C is determined with reference to the linear theory. It is worth noting that the above expression of the stability functional adopts the classical Green–Lagrange strain measure formulation specialized to the case of small strains and large rotations valid for thin bodies, and Eulero-Bernoulli beam kinematical assumptions.

In the stability functional Eq. (8) v and w denote the transverse and axial displacements for both girder and pylons and the meaning of other symbols are illustrated in Fig. 3. The first integral in Eq. (8) corresponds to the girder and contains the stabilizing effects of girder flexural (EI) and axial stiffnesses (EA) and the instabilizing geometrical effect due to axial compression N, respectively. The second term represents the analogous term relative to the left (L) and right (R) pylons containing both stabilizing stiffness and instabilizing geometrical terms. The third and fourth terms refer to the stabilizing effects of the n_L and n_R stays attached to the left and right pylons, respectively. The cross section area of the i-th stay is denoted by A_{si}. The last two terms in Eq. (8) are related to the stabilizing effects of anchor stays. Moreover, the deformation increment produced by the additional displacements in both regular and anchor stays is, respectively,

$$\delta\varepsilon_{L/R} = \frac{\delta v + \delta w_p}{H}\sin^2\alpha \pm \frac{\delta w - \delta v_p}{H}\sin\alpha\cos\alpha,$$

$$\delta\varepsilon_{0L/R}\frac{\delta w_p}{H}\sin^2\alpha_0 \mp \frac{\delta w - \delta v_p}{H}\sin\alpha_0\cos\alpha_0,$$

where $\pm$ applies to the left or right pylon, respectively. The contributions arising from the stays nonlinear response can be obtained by considering the following second order approximation of the stay strain energy increment:

$$\begin{aligned}\Delta W_{stay} &= \frac{A_{Si}H}{\sin\alpha}\int_0^{\delta\varepsilon} E_s^*(\Delta\varepsilon)d\Delta\varepsilon \\ &= \frac{A_{Si}H}{\sin\alpha}\int_0^{\delta\varepsilon}\left(E_0^* + E_1^*\Delta\varepsilon + E_2^*\Delta\varepsilon^2 + \cdots\right)d\Delta\varepsilon \\ &= \frac{1}{2}\frac{A_{Si}H}{\sin\alpha}E_t^*\delta\varepsilon^2 + \cdots\end{aligned}$$

where E_t^* is intended to be evaluated at the corresponding stress level σ_0 in each cable acting in the examined bridge equilibrium configuration.

It results that bridge stability is mainly a consequence of two competing nonlinear effects the instabilizing one of axial compression in both the girder and pylons and the stabilizing one due to the tangent stiffness of stays attached to the left and right pylons. The former one generally increases with the load parameter λ, the latter may increase or decrease depending on the actual deformed configuration of the bridge due to the softening cable behavior under shortening.

This effect can be shown by considering the curve of the tangent modulus of a cable stay versus the σ_0 representing the stress in the current equilibrium configuration whose stability is evaluated. The tangent modulus may decrease drastically when the current stress in the cable decreases due to shortening of the cable, especially for cables having

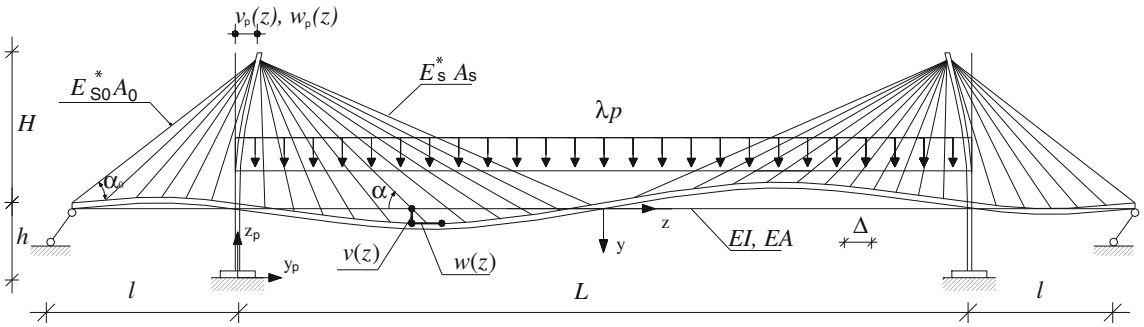

Fig. 3 In-plane scheme of the cable stayed bridge for the stability analysis

a large horizontal projection, approaching theoretically zero for a vanishing stress (see [6], for instance). Specifically with reference to the nonlinear bridge behavior envisaged in Fig. 2, the equilibrium is stable up to the snapping load since as the load parameter increases while in the central span the instabilizing effect of the axial compression is balanced by the stiffening stays in the lateral spans stays may show a large stress reduction produced by the lateral spans deflection and an instability condition is rapidly reached producing a bound in the applied load.

The characteristics of the nonlinear behavior of the cable stayed bridge structural system illustrated in this section, which strongly depend on the model adopted to account for non-linear cable response, will be clarified in the next section by considering a simple discrete model. These results will be rigorously confirmed by means of numerical results in the following sections.

2.2 An introductory example

The essential characteristics of the buckling and postbuckling behavior of the cable stayed bridge structural system can be illustrated with remarkable verisimilitude with reference to a one degree of freedom model consisting of two vertical rigid rods of length L, fixed in translation at the left end and free to translate in the horizontal direction at the right one, elastically constrained against vertical translation by two springs whose nonlinear stiffness coefficients are $k^1(\delta)$ and $k^2(\delta)$.

In presence of an horizontal load λ applied as shown in Fig. 4, the sequence of buckled states is represented by $\lambda = [k^1(\delta) + k^2(\delta)]\cos\alpha(L/2)$. The initial postbuckling equilibrium path can be expressed by the following asymptotic expansions: In the neighborhood of $\delta = 0$ the following asymptotic expansions are valid:

$$\begin{aligned} &\lambda = \lambda_c + \lambda_1\xi + \lambda_2\xi^2 + \cdots, \\ &k^i(\delta) = k_0^i + k_1^i\xi + k_2^i\xi^2 + \cdots, \quad i = 1,2, \end{aligned} \tag{9}$$

where $\xi = \delta/L$. It is assumed that $|k_1^1| > k_1^2 > 0$ and that $k_0^1 = k_0^2 = k_0$.

Considering that $\cos\alpha = \sqrt{1-\xi^2} = 1 - \xi^2/2 + \cdots$ and imposing that terms of the same power must vanish separately gives the critical load at which the bifurcated equilibrium path intersects the fundamental path, and the higher order coefficients of the load expansion:

$$\lambda_c = \frac{(k_0^1 + k_0^2)L}{2},\ \lambda_1 = \frac{(k_1^1 + k_1^2)L}{2},\ \lambda_2 = \frac{(k_2^1 + k_2^2)L}{2} - \frac{(k_0^1 + k_0^2)}{4L}.$$

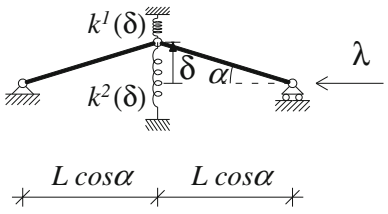

Fig. 4 Discrete model used to illustrate the buckling and postbuckling bridge behavior

If the spring response simulates the secant modulus model (the most accurate in this framework), by comparing Eqs. (9) and (5) with ξ playing the role of Δε, we obtain that $k_1^1 < 0$ while $k_1^2 > 0$ and $k_2^i > 0$, i = 1,2, since Δε is positive for a stay elongation. As a consequence, the first order coefficient of the load expansion λ_1 as well as the second one λ_2, become negative and an asymmetric bifurcation occurs at a load level $\lambda_c = k_0 L$.

On the contrary, when the spring stiffness coefficients are constant, namely k_0^i is the only non-zero term in the stiffness expansion, thus reproducing the constant tangent model for the stay behavior $\Delta\sigma/\Delta\varepsilon = E_t^*$, then a symmetric initial bifurcation occurs with $\lambda_1 = 0$ and $\lambda_2 < 0$ at the same load level of the secant modulus model.

Finally when the spring stiffness coefficients are constant ($k_1^i = k_2^i = 0$) and vanish for shortening according to the following expressions:$k_0^1 = k_0(1 - sign(\delta))/2$, $k_0^2 = k_0(1 + sign(\delta))/2$,where sign denotes the signum function, the tension only model is reproduced and a symmetric bifurcation also occurs but at a critical level $\lambda_c = k_0 L/2$ significantly lower than the tangent modulus case.

The actual behavior of the structure can be obtained by introducing initial imperfections and is characterized by a snap buckling behavior in the tangent and tension only models for imperfections of either signs, whereas in the case of the secant model only for positive imperfections, as illustrated in Fig. 5.

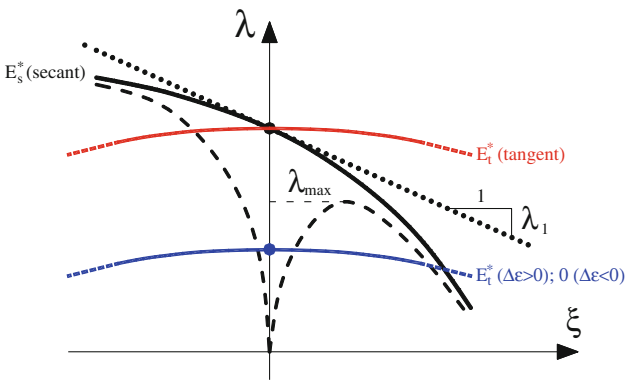

Fig. 5 Buckling behavior of the discrete model for different stay response models

3 Model formulations

In this section firstly an equivalent continuous model of the bridge is briefly introduced assuming a continuous distribution of the stay stiffness along the girder. This simplified model allows to point out the main parameters governing the non-linear behavior of the bridge to be used in the subsequent more general analysis adopting a 3D nonlinear finite element discrete bridge model, corresponding to the actual stays spacing.

3.1 Continuous bridge model

In this section a continuous model for the analysis of the static response of cable stayed bridges is presented based on a diffuse stays arrangement ($\Delta/L \ll 1$). The proposed model is able to predict the static behavior of cable stayed bridges taking into account the nonlinear behavior of the single stay, adopting the Dischinger's fictitious secant modulus for the cables to model the stays nonlinear behavior and including the instability effect due to the axial compression in the girder. The analyzed bridge scheme is illustrated in the Fig. 6. The stays are fan shaped with constant spacing Δ. The girder is supported by stays joining at the tower tops. The two lateral couple of stays, called anchor stays, assure the bridge equilibrium and are anchored by means of two vertical supports; the girder is not constrained in the longitudinal direction.

It is assumed that the erection method is such that the deck's final configuration is practically straight and free from bending moments [12, 25]. The bridge static response when the live load λp increasing with the parameter λ is applied, is now considered starting from the straight equilibrium configuration of the bridge's deck corresponding to the application of the dead load g and cables pre-stress. The cable stayed bridge deformation is defined by the following displacement parameters:

- The function $v(z)$ which represents the girder's vertical displacements;
- The girder's horizontal displacement $w(z)$;
- The pylon tops horizontal elastic displacement u;
- The girder's torsional rotations $\theta(z)$;
- The pylon tops torsional rotation ψ.

As a matter of fact, the horizontal equilibrium of the bridge requires shear forces to be the same at the pylon top sections and this ensures that displacements of the pylon tops will always be equal and opposite. Similarly due to rotational equilibrium considerations about the y-axis, the pylon tops torsional rotations will always be equal and opposite.

The vertical, horizontal and torsional equilibrium equations for the girder respectively are:

$$\begin{aligned} &EIv^{IV} + \left[(N^g + \Delta N(w))v'\right]' - q_v = \lambda p \\ &EAw^{II} + q_h = 0 \\ &C_t\theta^{II} = -m_t - \lambda pe, \end{aligned} \tag{10}$$

where the prime denotes differentiation with respect to z, EI is the girder flexural stiffness, N^g represents the axial force in the girder due to the dead load g:

$$N^g(z) = gH/2\left[(L/(2H))^2 - (z/H \pm L/(2H))^2\right], \tag{11}$$

$\Delta N(w) = EAw'$ indicates the axial force increment in the girder due to live loads, E, A and C_t are respectively the Young modulus, the cross section area and the torsional stiffness for the girder. Moreover $q_v$is the vertical component of the stays-girder interaction, whereas $q_h$denotes the horizontal component of the stays-girder interaction. The two components of the stays-girder interaction depend on E^*_{SL} and E^*_{SR}, representing the Dischinger's secant modulus for the cables, respectively applied on the left (L) and on the right (R) stays with respect to the y–z plane (see the right of Fig. 6). Note that E^*_{SL} and E^*_{SR} depend on the additional axial strain $\Delta\varepsilon$ in the cables produced by the additional displacements v, w, u, θ and ψ and that the initial stress of Eq. (2) here represents the stress in the cables under the dead loads g. In Eq. (10) m_t denotes the torsional couple per unit length.

Usually the stays cross section area A_s of the left or right curtains of stays is designed so as dead loads produce constant tension in all stays and this leads to $A_S = g\Delta/(2\sigma_g sin\alpha)$ in which σ_g is defined as a function of the allowable stress σ_a as $\sigma_g = g\sigma_a/(p + g)$ by assuming that the stress increment in the stays are proportional to the design live loads p. For the anchor stays the cross sectional geometric area A_0 is designed in such a way that the allowable stress σ_a is obtained for live loads p applied to the central span only, leading to:

$$A_0 = gl/4\sigma_{g0}\left[1 + (l/H)^2\right]^{1/2}\left[(L/(2l))^2 - 1\right]. \tag{12}$$

where the initial tension σ_{g0} in the anchor stays is equal to:

$$\sigma_{g0} = \sigma_a\left[1 + \frac{p}{g}\frac{(L/(2l))^2}{(L/(2l))^2 - 1}\right]^{-1}. \tag{13}$$

The horizontal and torsional equilibrium equations for the pylons, involving the effects of the stays-girder interaction, should lead to integral equations. In order to write the horizontal equilibrium equation for the left pylon in a differential form, a fictitious rigid beam is considered on which the horizontal component of the stays-girder interaction is applied only for the left part of the bridge (see also [25]). The towers stiffness is distributed over the fictitious rigid beam for the entire span of the bridge. Consequently, the horizontal left pylon equilibrium equation assumes the following expression:

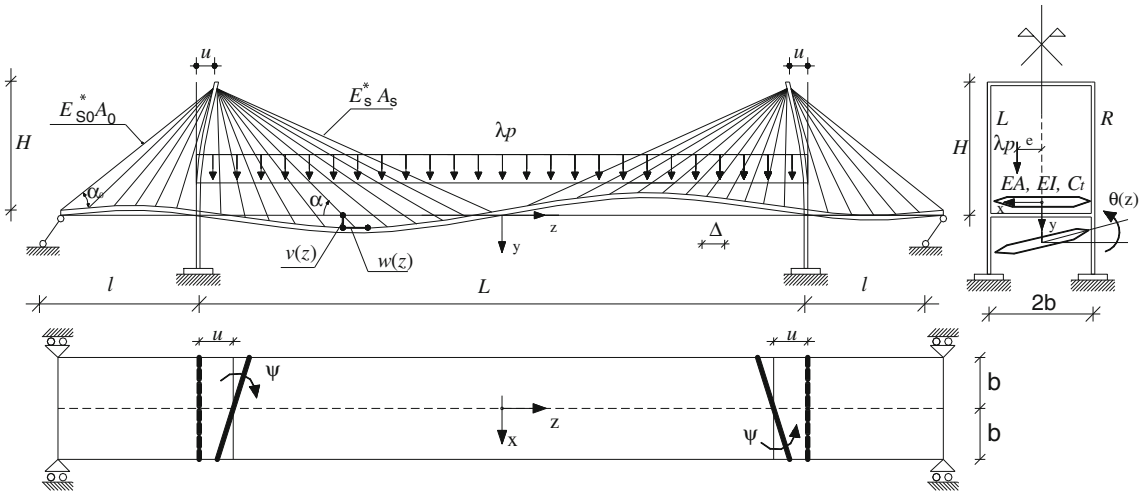

Fig. 6 The long-span cable stayed bridge structural scheme

$$K_u u^{II} - q_h - \frac{Ku}{(L+2l)} = 0, \tag{14}$$

where K_u and K are respectively the fictitious beam axial stiffness and the pylon tops flexural stiffness. In particular, in numerical simulations K_u, acting as a penalty stiffness parameter assumes a very large value but not too large to avoid numerical complications. Note that in Eq. (14) the horizontal component of the stays-girder interaction q_h vanishes on the right side of the bridge ($z > 0$).

Similarly for the torsional equilibrium of the left pylon a penalty flexural stiffness parameter K_ψ, representing the torsional stiffness of a fictitious rigid beam, is considered leading to the following torsional equilibrium equation for the left pylon:

$$K_\psi \psi^{II} - m_f - \frac{Kb^2\psi}{(L+2l)} = 0, \tag{15}$$

where m_f is the horizontal flexural couple acting on the left side of the bridge ($z < 0$). Solutions for the differential Eqs. (10), (14) and (15) are obtained imposing the appropriate boundary conditions. With reference to the girder vertical equilibrium the associated boundary conditions require that the girder vertical displacement and the curvature vanish at both $z = -L/2 - l$ and $z = L/2 + l$. Analogously with reference to the girder torsional equilibrium the associated boundary conditions require that the girder torsional rotations vanish at both $z = -L/2 - l$ and $z = L/2 + l$.

The two boundary conditions associated with the horizontal equilibrium of the left pylon impose that at the left edge of the fictitious rigid beam $K_u u^I$ is equal to the resultant horizontal component S_0 of the anchor stays axial forces, whereas at the right edge $K_u u^I$ vanishes. The two boundary conditions related with the torsional equilibrium of the left pylon impose that at the left edge of the fictitious rigid beam $K_\psi \psi^I$ is equal to the torsional moment M_0 associated to the horizontal components of the anchor stay axial forces and that at the right edge $K_\psi \psi^I$ vanishes. The boundary condition related to the horizontal equilibrium of the girder, requires that the axial force is compatible with the resultant horizontal component of the anchor stays axial forces.

In order to analyze the main parameters governing the differential problem the above equations can be rewritten in a dimensionless form. To this end the following dimensionless quantities are introduced:

$$\zeta = \frac{z}{H}, \quad V = \frac{v}{H}, \quad U = \frac{u}{H}, \quad W = \frac{w}{H}, \quad \xi = \frac{e}{b}, \quad t = \frac{b}{H},$$
$$a = \frac{\gamma^2 EH^2}{12\sigma_g^3}, \quad \varepsilon = \sqrt[4]{\frac{4I\sigma_g}{H^3 g}}, \quad \varepsilon_A = \frac{A\sigma_g}{Hg}, \quad \tau = \sqrt{\frac{C_t\sigma_g}{Eb^2 Hg}}. \tag{16}$$

The parameters ε, ε_A and τ, respectively represent a measure of the relative bending, axial and torsional stiffness between the girder and stays, whereas a is related to the stay deformability accounting for the cable sag effect. Additional details on the continuum bridge formulation can be found in [12, 25–32]. It is worth noting that the above formulation does not take into account for buckling in the horizontal plane (out-of-plane buckling) and is strictly valid for the H-type pylon shape. These restrictions will be removed in the more general discrete bridge model.

The boundary value problem, governing the equilibrium of the long-span cable stayed bridge, can be reformulated as a non-linear system of first order ordinary differential equations subject to boundary conditions only at two-points. This transformation technique causes an increase of

the variables number. In particular, as far as the in-plane case is considered (namely $\theta(z) = \psi = 0$) the unknown variables, defined in the dimensionless integration domain $[-r_1 - r_2, r_1 + r_2]$ in which r_1 is equal to $L/2H$ and r_2 is equal to l/H, are $[V, V^I, V^{II}, V^{III}, V^{IV}, U, U^I, W, W^I]$. The reformulated boundary value problem assumes the form:

$$\boldsymbol{y}'(\xi) = \boldsymbol{g}(\boldsymbol{y},\xi), \quad -r_1 - r_2 \le \xi \le r_1 + r_2 \tag{17}$$

where $\boldsymbol{y} = [y_1, y_2, y_3, y_4, y_5, y_6, y_7, y_8]$ is a vector of the unknown functions of the problem (collecting displacement parameters and their derivatives) and $\boldsymbol{g}$ is an opportune vector function.

In Eq. (17) the prime denotes differentiation with respect to ξ. Equation (17) is subjected to the two-points linear boundary conditions:

$$\boldsymbol{B}_0\boldsymbol{y}(0) + \boldsymbol{B}_1\boldsymbol{y}(1) = \boldsymbol{c} \tag{18}$$

where $\boldsymbol{B}_0$ and $\boldsymbol{B}_1$ are opportune matrices containing coefficients of boundary and matching conditions and $\boldsymbol{c}$ is an opportune known vector. The boundary value problem has been solved by means of an iterative collocation method implemented in MATLAB which provides a $C1$-continuous solution by using a cubic collocation polynomial on each subinterval of the mesh. Starting from an initial guess for the solution and the mesh, at each iteration the method adapts the mesh to obtain a sufficiently accurate numerical solution. Preliminary convergence analyses carried out for increasing values of the penalty parameter K_u, have shown that assuming a value equal to $EA \times 10^5$ ensures that the displacement function u practically assumes a constant value over z with reasonably small errors related to the approximation of the fictitious rigid beam behavior. On the contrary, increasing further the penalty parameter leads to numerical convergence problems in the adopted integration scheme.

3.2 Discrete FE bridge model

In the present subsection a 3D discrete bridge model is examined with reference to the actual stays spacing, taking into account the geometric nonlinear effects for the cable system under general loading conditions, in order to obtain more accurate results and to assess the limit of validity of the continuous model. In the discrete model all the restrictions placed on the continuum model, such as those regarding the continuous distribution of stays, the axial deformability of pylons and the initial configuration under dead loads, have been removed.

This discrete model has been studied by means a displacement-type finite element (FE) approximation, implemented in the commercial software COMSOL MULTIPHYSICS™ [33]. In order to reduce the computational effort in the numerical calculations, a three dimensional finite element model has been developed by using beam elements for the girder and the pylons and nonlinear truss elements for the cable system. Specifically, the bridge deck is replaced by a longitudinal spline with equivalent sectional and material properties and the pylons are composed by two columns connected at their top and at the level of the bridge deck by two horizontal beam elements. In the case of the A-type pylon shape the length of the beam connecting the tops of the columns approaches zero, whereas in H-type case both the upper and lower horizontal beams have the same length.

Moreover, the instabilizing effects produced in both girder and pylons by the axial compression force induced by stays and due to the girder loading $g + \lambda p$ has been accounted by adding the following weak contributions for the girder and pylons, respectively, to the virtual work principle formulation:

$$-\left(\int_{L_e} N\theta_y\delta\theta_y\,dL + \int_{L_e} N\theta_z\delta\theta_z\,dL\right),$$
$$-\left(\int_{L_e} N\theta_y\delta\theta_y\,dL + \int_{L_e} N\theta_x\delta\theta_x\,dL\right)$$

where N is the axial force, θ_y, θ_z and θ_x denote the bending rotation about the y, z and x axes, and L_e is the element length (Fig. 7).

The cable system is modeled according to the multi element cable system (MECS) approach, where each cable is discretized using multiple truss element. The stiffness reduction caused by sagging is accounted for by allowing the cable to deform under applied loads. Large deformations are accounted by using Green–Lagrange strains and the axial strain is calculated by expressing the global strains in tangential derivatives and projecting the global strains on the cable edge. Additional details about the approach here adopted to model nonlinear cable behavior can be found in [28, 33]. It is worth noting that different approaches have been proposed in the literature to model the nonlinear cable behavior ranging from the simple equivalent modulus approach, according to which each cable is replaced by one bar element characterized by an equivalent tangent modulus [8, 17] often with a tension only behavior [5, 6, 9, 14, 16], to more accurate techniques based on exact analytical expressions for the elastic catenary [34]. Between these two approaches, alternative techniques have been proposed such as to divide each cable into several truss elements to adequately model the curved geometry of the cable or to use isoparametric elements. Moreover, quasi-secant and refined models for cable constitutive law have been proposed in [35, 36] able to determine approximate closed-form solution of the statical

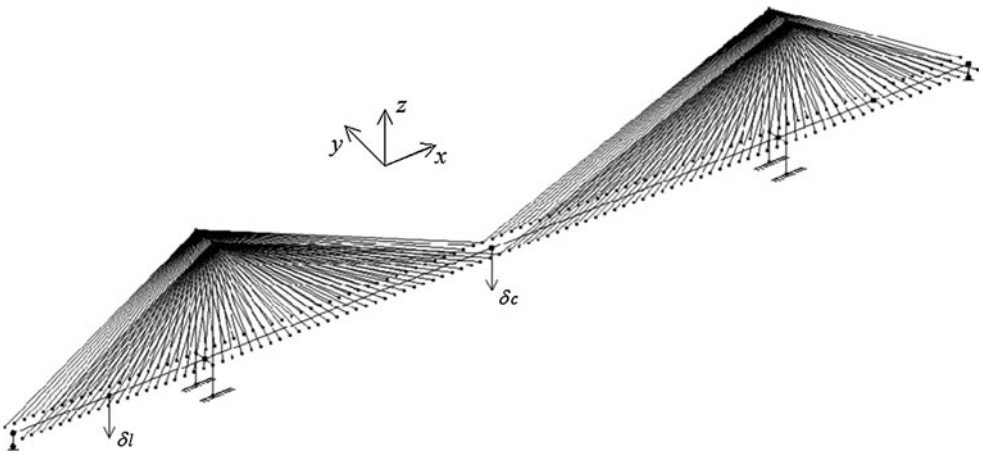

Fig. 7 The finite element model of the bridge

cable-stayed bridge problem, whereas cables have been modelled in the context of continuous formulation as one bar elements adopting the Dischinger secant modulus to investigate the dynamic response of cable-supported bridges under moving loads [27] or the aeroelastic stability problem of long-span cable-stayed bridges [37]. Additional applications of numerical nonlinear cable modelling techniques can be found in [38, 39].

In the case of the simplified cable behavior simulated by using the tangent modulus, a single truss element is adopted for each stay and the geometrical nonlinearities are deactivated. The constitutive behavior is simulated by introducing the expression shown in Eq. (3) for the truss element constitutive modulus, with the initial stress derived from results obtained through the initial shape analysis formulated in the sequel.

The tension only behavior is modeled similarly except that a nonlinear constitutive behavior according to Eq. (4) is incorporated in the constitutive relationship of the truss element representing the single stay. To this end the longitudinal modulus of the truss element is multiplied by a step function depending on the axial strain increment with respect to the initial configuration of the bridge under dead loading, in order to exclude any stiffness contribution of the cable under shortening. Therefore, the constitutive behavior of the truss element is:

$$\Delta\sigma = E_t^* step(\Delta\varepsilon)\Delta\varepsilon, \quad step(\Delta\varepsilon) = \begin{cases} 1 & \text{if } \Delta\varepsilon \geq 0 \\ 0 & \text{if } \Delta\varepsilon < 0 \end{cases}.$$

In order to avoid numerical convergence complications related to the bimodular constitutive behavior of the tension only model, an appropriate regularization is adopted for the step function. To this end the a smoothed step function available in [33] is adopted approximating the discontinuous step function by smoothing the transition within the interval $-10^{-5} < \Delta\varepsilon < 10^{-5}$. In the interval $-10^{-5} < \Delta\varepsilon < 10^{-5}$ the smoothed function is defined by a 7th-degree polynomial chosen so that the derivatives up to the 2nd order are continuous and that the functions have small overshoots. The constraint condition between the girder and the stays is modeled with offset rigid links to accommodate cable anchor points, by means of the extrusion coupling variable methodology (see [33] for additional details). Briefly, once the displacement field of the 3D beam (u, v, w, θ_x, θ_y, θ_z) is linearly extruded from the source domain (the stiffening girder) to the destination ones (the lines which contain anchor points), prescribed displacements are imposed as constraint on the destination domains, by means of the following constraint equations:

$$\begin{aligned} &\bar{u}^{(l)} = u + \theta_z b; \quad \bar{v}^{(l)} = v; \quad \bar{w}^{(l)} = w + \theta_x b; \\ &\bar{u}^{(r)} = u - \theta_z b; \quad \bar{v}^{(r)} = v; \quad \bar{w}^{(r)} = w - \theta_x b \end{aligned} \tag{19}$$

where $\bar{u}^{(l)}, \bar{v}^{(l)}, \bar{w}^{(l)}$ and $\bar{u}^{(r)}, \bar{v}^{(r)}, \bar{w}^{(r)}$ are the prescribed displacements on left and right anchor point, respectively. A regular mesh is used to obtain the discrete model: each cable stay is divided in twenty linear truss elements, whereas 350 beam elements are used to discretize the stiffening girder.

The bucking and post-bucking behaviors have been investigated by using nonlinear analyses taking into account large deformation but small strains with linear stress–strain relationship and a solution strategy based on the damped Newton method has been adopted. A suitable modeling technique in this case, where the relationship between applied loads and displacements is highly nonlinear, is to use an algebraic equation that controls the applied live loads λp so that the generalized deflection of a control point reaches the prescribed values. In order to capture the typical snapping behavior of the load–displacement curve, a generalized deflection increasing monotonically with the evolution of the loading process is adopted, so that no snap-backs are detected when the load–displacement curve is plotted in terms of the assumed control parameter. In the case of loading on the central span of the bridge, an appropriate choose to capture the snapping behavior is the lateral mid-span deflection δ_l or the girder end in-plane rotation θ_l, although in some cases relevant to the TO model the central

midspan deflection δ_c has been adopted. The ODE interface in COMSOL MULTIPHYSICS^{TM} is useful for entering this coupled algebraic equation, written as follows $\delta_l(\lambda) = \bar{\delta}_l^{(i)}$ where $\bar{\delta}_l^{(i)}$ is the desired vertical displacement stepped up by employing a parametric solver. In this way a displacement driven loading path is simulated able to describe the snapping behavior in the load–displacement curve.

The equilibrium configuration of the bridge under the action of dead load is characterized by large deflections and huge bending moments in both the girder and towers when no pretension exist in inclined cables, since the bridge span is large. To this end an initial shape analysis must be carried out to find the geometric configuration together with the associated pretension force distribution in cables satisfying both equilibrium and the design requirements of a straight initial bridge configuration.

All geometric nonlinearities are taken into consideration in the initial shape analysis, namely geometric effects of axial compression in both girder and towers and cable sag nonlinearties induced by cable dead load. The correct initial shape of the cable stayed bridge, reducing the deflections and smoothing the bending moment in the girder, is determined by adding a set of coupled equations in the finite element model imposing that vertical displacements at the nodes intersected by the girder and the cable v_{i} (control points) and horizontal displacements at the tip of the towers u (node intersected by the towers and cables) vanish within a given tolerance:

$$\begin{cases} u(N_1^0, \ldots, N_n^0) = 0 \\ v_i(N_1^0, \ldots, N_n^0) = 0 \quad i = 2, \ldots, n \end{cases}, \tag{20}$$

where the unknowns $N_1^0, \ldots, N_n^0$ represent the pretension forces in the double curtain of stays and the analysis is restricted to one half of the bridge due to symmetry.

The initial shape nonlinear optimization has been performed by using the ODE interface of COMSOL which adds global equations to the model. In order to improve converge performance trial initial cable forces are estimated by means of the balance of vertical loads related to the initial truss like behavior in the continuous model. Both equilibrium and shape iterations have been performed by adopting a numerical solving procedure based on the Newton–Raphson method.

In both the cases of the tangent and tension only models the initial shape analysis is carried out by using geometrically linear truss elements.

4 Numerical results

Here numerical results for both the continuous model and the discrete one are presented to examine the instabilizing effect produced by the axial force in the girder for increasing live loads λp for different loading conditions, geometrical configurations and pylon shapes. Two types of loadings are considered: a uniform load distributed on the whole bridge length and a uniform load applied on the central span only. Moreover, both the H-type and A-type pylon shapes are analyzed and different eccentricities with respect to the deck axis of the live load are taken into account.

In the case of the continuous model results are limited to an in-plane analysis and to the case of uniform load applied on the central span. As a matter of fact this bridge model is useful to determine the main geometrical and mechanical parameters governing the bridge behavior which will be used in the more general 3D analysis using the discrete model in order to perform a useful parametric analysis.

The following dimensionless parameters are used in the numerical analyses related to the continuum model, unless otherwise stated: $\frac{L}{2H} = 2.5$, $\frac{l}{H} = 5/3$, $\frac{b}{H} = 0.1$, $\frac{\Delta}{L} = 1/105$, $\frac{\sigma_a}{E} = 7200/2.1 \times 10^6$, $\frac{K}{g} = 50$,,whereas the material properties assume the values that concern the usual case of steel girders and towers. The value of the dead load g is equal to 300,000 N/m, typical of a steel deck, whereas the cable unit volume weight has been assumed equal to $\gamma = 77.01$ kN/m^3.

The other parameters ε, ε_A and a are used to define the bridge geometrical parameters according to the following formulas:

$$H = \sqrt{\frac{12a\sigma_g^3}{\gamma^2 E}}, \quad I = \frac{\varepsilon^4 H^3 g}{4\sigma_g}, \quad A = \frac{\varepsilon_A H g}{\sigma_g}.$$

Moreover, the ratio between live load p and dead load g is adopted to determine the stays cross section as shown in Sect. 3. A parametric analysis is carried out by adopting the following values for the above quantities: $\varepsilon = 0.2$ or 0.3, $a = 0.10$ or 0.20 and $p/g = 0.5$ or 1, whereas ε_A has been assumed equal to 54.5.

As far as the analysis carried out with the discrete model is concerned, the following additional parameters are needed:

$$\varepsilon_h = \sqrt[4]{\frac{4I_{zz}\sigma_g}{b^3 g}}, \quad I_r = \frac{I_{pyy}}{I},$$

defining respectively the relative girder to stay stiffness for bending in the horizontal plane and the tower to girder bending stiffness ratio for bending in the vertical plane. The former parameter gives the bending stiffness EI_{zz}, whereas the latter the pylon bending stiffness $EI_{p\ yy}$. The towers stiffness $I_{p\ xx}$ for out-of-plane bending has been assumed equal to $EI_{p\ yy}$ and the ratio between the height of the pylon from pier bottom to bridge deck H_1 and H has been assumed equal to 0.25. The axial, bending and

torsional stiffnesses of the beams connecting the two towers of the pylons have been assumed equal to the corresponding ones adopted for the towers. Moreover the cross section area and the torsional stiffness of the towers have been assumed equal to those of the girder. These parameters allow to define the bridge characteristics for the 3D discrete model. Additional parametric analyses are carried out with reference to I_r and ξ by adopting the following ranges of variation: $\xi = 0 \div 0.75$, $I_r = 0.5 \div 70$. On the other hand the following values have been assumed for the remaining parameters: $\tau = 0.1$, $\varepsilon_h = 5$, $t = 0.1$. In the analyses carried out exclusively with the discrete model a larger value of Δ/L has been chosen equal to 1/60, whereas the comparisons between the discrete and continuum models have been made by assuming $\Delta/L = 1/105$.

For instance, in the case of $p/g = 1$, $\varepsilon = 0.2$, $a = 0.1$, $Ir = 50$, $\Delta/L = 1/60$, $\xi = 0.75$, $\tau = 0.1$, the above assumptions for the dimensionless parameters leads to $L = 1{,}040$ m, $l = 346.7$ m, $H = 208$ m, $H_1 = 52$ m, $e = 15.6$ m, $\Delta = 17.33$ m, $b = 20.8$ m, $A_o = 0.5$ m^2, $A = 9.63$ m^2, $I = 3.06$ m^4, $I_{zz} = 1{,}194.5$ m^4, $C_t = 1.57 \times 10^{11}$ Nm^2, $I_{pyy} = I_{pxx} = 152.90$ m^4, $\sigma_g = 3.53 \times 10^8$ N/m^2, $\sigma_{g0} = 2.52 \times 10^8$ N/m^2, $E = 2.06 \times 10^{11}$ N/m^2.

4.1 Comparisons between the continuous and discrete models

The case of uniform load applied on the central span is considered to compare results obtained by using the continuum and the discrete models. In the sake of simplicity, the analysis does not involve out-of-plane displacements and the in-plane instabilizing effect produced by the axial force in the girder for increasing live loads λp is investigated. In accordance with the approximations introduced by the continuum model, in the discrete model the axial deformability of the pylons has been neglected and only geometrical nonlinearities in the girder are modeled.

Table 1 shows the influence of bridge parameters on the maximum load parameter λ_{max} for both the continuous and discrete model. The influence of stays geometric nonlinearities is also pointed out by computing load maximum when the tangent modulus linear model (denoted as LM in Table 1 in contrast with NLM used when geometrical nonlinearities are accounted) is adopted for the stays response with E_t^* assumed equal to E (i.e. $\sigma_0 \to \infty$). In the case of the continuum model geometrical nonlinearities in the stays are accounted by using the secant modulus model [Eq. (2)], whereas in the discrete model the multiple truss element formulation has been used. Results show the strong influence of the girder stiffness parameter and of the p/g ratio, the former being stabilizing and the latter destabilizing. Moreover the increase of the stays deformability parameter a has a detrimental effect on the maximum load. The continuous model gives reasonably accurate results with respect to the discrete model, with a maximum underestimation of the load maximum of about 9 % when stays geometrical nonlinearities are accounted and a maximum overestimation of about 5 % when the linear tangent model is adopted. It turns out that in the more accurate case when the stays geometrical nonlinearities are considered, the continuous model is able to provide conservative predictions of the maximum load carrying capacity. Moreover, the above comparisons show that the simplified continuous model is able to capture the main features of the cable stayed bridge nonlinear response. This confirms the validity of the parametric analysis which will be carried out in the sequel with reference to the discrete model, based on the dimensionless parameters derived from the theoretical analysis carried out by using the continuous model.

4.2 Influence of stays response modeling on the nonlinear bridge response

The analysis will be now devoted to investigate the influence of the different stays response approaches introduced in Sect. 2, on the bridge nonlinear behavior by using the more general 3D discrete model. To this end the response of a single stay has been modeled by using the multiple truss element nonlinear formulation, which will be denoted as NLM, the tangent modulus linear model (denoted as LM in the sequel) which adopts Eq. (3) with the initial stress derived from the initial shape analysis and the tension only approximation introduced by Eq. (4) (denoted as TO in the sequel). The influence of the three stays response models has been analyzed for different values of ε and a and for both the case of central loading and uniform loading on the whole bridge length. Moreover, both A and H pylon shapes have been considered.

Figure 8 shows for $\varepsilon = 0.2$ and 0.3, $a = 0.2$ and $p/g = 1$ the typical snapping for high values of λ due to the coupling between the instabilizing effect of the axial compression in the girder and the softening behavior of stays response in the lateral span, occurring in the case of the central loading condition and the H pylon shape. This behavior is represented in term of the load parameter versus central midspan deflection δ_c. As the load parameter increases while in the central span the instabilizing effect of the axial compression is balanced by the stiffening stays in the lateral spans stays show a large stress reduction produced by the lateral spans deflection and an instability condition is rapidly reached producing a bound in the applied load. The load–displacement curves are represented in term of the central midspan deflection δ_c in order to better appreciate the differences between the three

Table 1 Influence of the parameters ε, *a* and *p/g* on the maximum load parameter λ_{max} in both the cases of nonlinear (NLM) and linear (LM) approaches and for both continuous (C) and discrete (D) models

	λ_{max}								
	a	0.10				0.20			
	ε	NLM (C)	NLM (D)	LM (C)	LM (D)	NLM (C)	NLM (D)	LM (C)	LM (D)
$p/g = 0.5$	0.2	2.39	2.58	4.11	3.96	2.18	2.37	4.11	3.90
	0.3	5.30	5.57	9.69	9.50	5.35	5.39	9.69	9.42
$p/g = 1$	0.2	1.61	1.74	2.88	2.81	1.48	1.63	2.88	2.78
	0.3	3.44	3.49	6.53	6.44	3.32	3.39	6.53	6.41

considered models, although the nonlinear analyses have been driven always by the lateral midspan deflection. The corresponding evolution of bridge deformed shape for the NLM model with ε = 0.2 is illustrated in Fig. 9 with reference to the three loading levels shown in Fig. 8a. The evolution of the bridge deformation is shown by using a color map of the displacements. In Figs. 8 the results obtained by using the linear tangent model (LM) and the tension only model (TO), are also shown in order to appreciate the influence of the nonlinear cable response modeling on the global bridge behavior.

As expected in light of the theoretical developments given in Sect. 2, the load displacement diagrams for different girder stiffness parameters evidence a notable overestimation for the LM approach whereas an underestimation for the TO one with respect to the actual behavior (NLM).

The stress evolution of the lateral span central stay as function of the load parameter is shown in Fig. 10 for the different stays response models (NLM and LM). A large stress reduction is shown due to upward deflections in the lateral spans. It is worth noting that in the case of the LM approach compression is allowed.

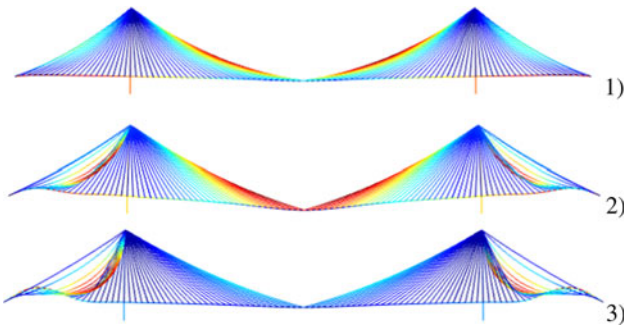

Fig. 9 Evolution of bridge deformed shape for the NLM model shown in Fig. 9a

A parametric analysis for different values of the parameters ε, *a* and *p/g* has been carried out and the results are summarized only in terms of the maximum load parameter in Table 2. These results show the strong stabilizing effect of the girder stiffness independently on the adopted model and confirm the considerations made on the basis of the load–displacement plotted of Fig. 8 about the underestimation of the TO model and the overestimation of the LM one. Moreover it can be noted that for the nonlinear

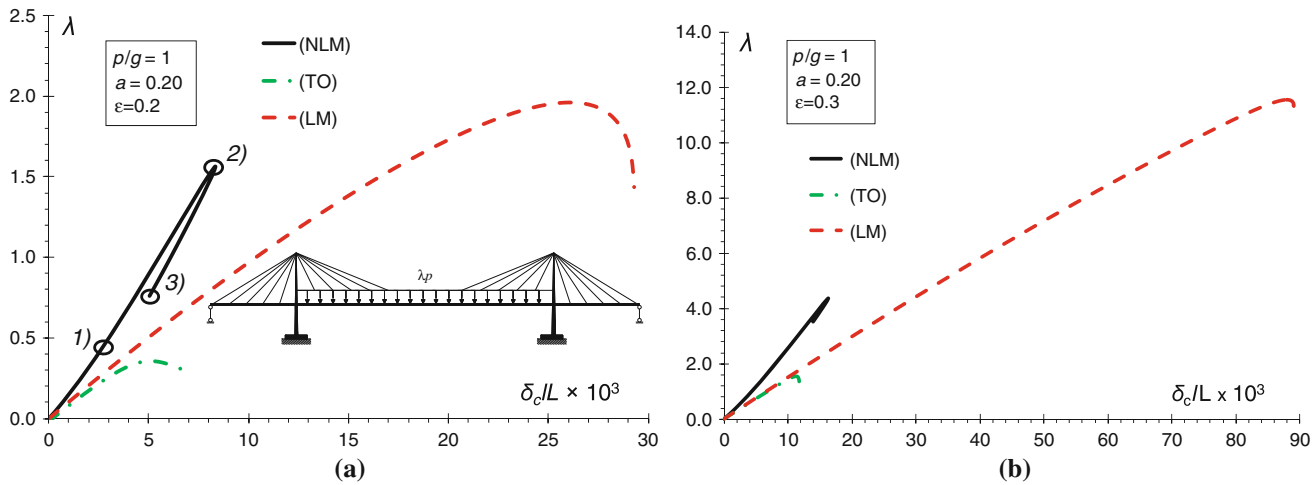

Fig. 8 Plots of the load parameter λ versus δ_c (central midspan deflection) for the central loading condition and H pylon shape: influence of the different stay response models for ε = 0.2 (**a**) and ε = 0.3 (**b**)

model increasing the stay deformability parameter a leads to a reduction of the limit load, although the effect of this parameter appears weaker than that related to the girder stiffness. This applies also to the linear and tension only models for the lower value of the girder stiffness parameter, whereas for the larger one an opposite effect takes place.

In the case of the uniform loading on the whole bridge length the nonlinear behavior is governed by the instabilizing effect of axial compression, while cables provide a stiffening effect except for a very small group of cables in the lateral span near the maximum load. The typical snap buckling behavior of the bridge is shown in Fig. 11 in term of the load parameter versus central midspan deflection δ_c.

Contrarily to the previous loading condition, as the load parameter increases the effect of softening in stays tangent stiffness is negligible occurring for a very small group of cables and for larger load level, and the stays are characterized by tensile axial strains except near the load maximum. The global behavior is characterized by a local maximum that is displayed near the end of the curve, being activated by the softening behavior of the small group of cables referred to above.

As a consequence the influence of the softening cable behavior under shortening is less appreciable with respect to the central loading case and the maximum load depends strictly on the nonlinear prebuckling effects which leads to larger displacements and rotations in the central span when the tangent modulus or the tension-only models are adopted.

The corresponding evolution of bridge deformed shape for the NLM model with $\varepsilon = 0.2$ is illustrated in Fig. 12 with reference to the loading level shown in Fig. 11a.

Also in the case of the uniform loading condition, the results obtained by using the linear tangent model (LM)

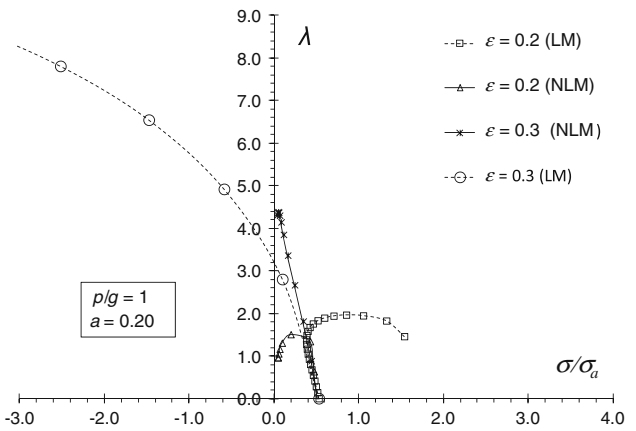

Fig. 10 Plot of σ (lateral span central stays stress) versus the load parameter λ for different values of ε in both the cases of nonlinear (NLM) and linear (LM) discrete model. Central loading condition and H pylon shape

Table 2 Influence of the parameters ε, a and p/g on the maximum load parameter λ_{max} for the nonlinear (NLM), linear (LM) and tension-only (TO) approaches in the context of the discrete FE model

	a	0.10			0.20		
	ε	NLM	LM	TO	NLM	LM	TO
$p/g = 0.5$	0.2	2.403	3.047	0.657	2.197	2.617	0.519
	0.3	7.109	14.156	1.218	6.910	15.669	1.252
$p/g = 1$	0.2	1.678	2.248	0.395	1.563	1.962	0.353
	0.3	4.476	9.918	1.370	4.380	11.534	1.537

Central loading condition and H pylon shape

and the tension only model (TO) are shown in order to appreciate the influence of the nonlinear cable response modeling on the global bridge behavior (see Fig. 11). However, in this case it is possible to appreciate the conservative behavior of the LM and TO models with respect to the NLM, in terms of the maximum load parameter λ_{max}.

Moreover, Fig. 11 shows how the LM and TO models are characterized by the same behavior, due to the fact that, in the case of the uniform loading condition, cables are always in tension except for a very small group of stays in the lateral span near the maximum load.

Also in this case, a parametric analysis for different values of the parameters ε, a and p/g has been carried out and the results, in terms of the maximum load parameter, are shown in Table 3. These results exhibit, like in the case of the central loading condition, the strong stabilizing effect of the girder stiffness independently on the adopted model and confirm the considerations, made on the basis of the load–displacement plotted in Fig. 11, about the overestimation of the NL model with respect to the LM and TO models.

It can be evidenced that for all the three models increasing the stay deformability parameter a leads to a reduction of the limit load, although the effect of this parameter appears notably weaker than that of the girder stiffness one.

In order to analyze the influence of the pylon shape on the global non-linear behavior of long-span cable stayed bridges, a parametric analysis for different values of the parameters ε, a and p/g has been carried out for the A pylon shape.

Results, summarized in the Table 4 (central loading condition) and Table 5 (uniform loading condition on the whole bridge length) only in terms of the maximum load parameter and for the NLM and LM models, are in agreement with those obtained for the H pylon shape.

This aspect is also confirmed by the comparison in terms of the typical snap buckling behavior of the bridge for the central loading condition, shown in Fig. 13 for the H-type and A-type pylon shape and for $\varepsilon = 0.2$, and shows how

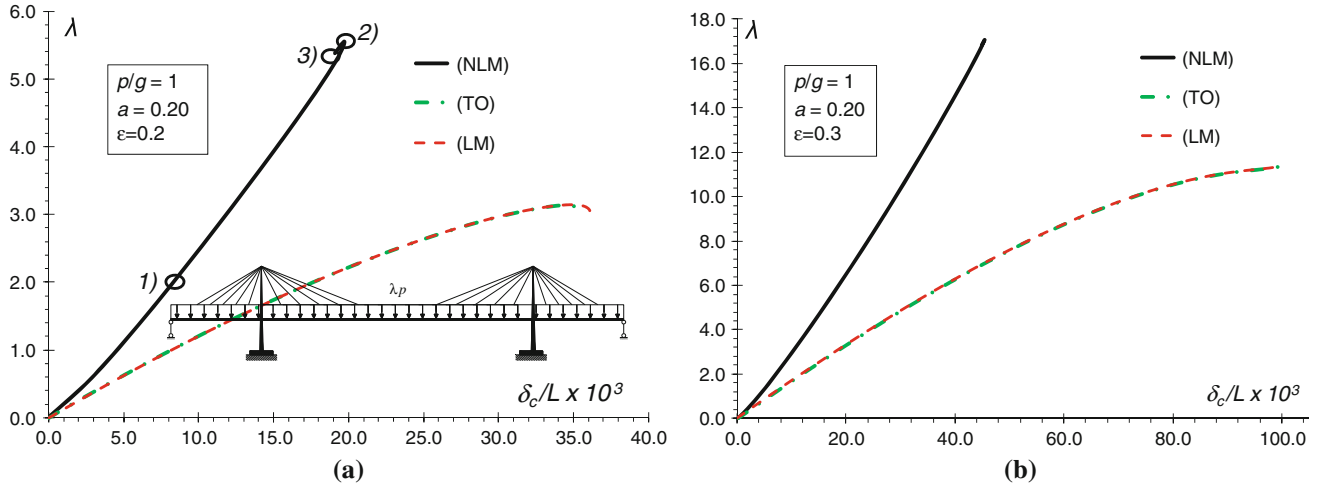

Fig. 11 Plots of the load parameter λ versus δ_c (central midspan deflection) for the uniform loading condition and H pylon shape: influence of the different stay response models for $\varepsilon = 0.2$ (**a**) and $\varepsilon = 0.3$ (**b**)

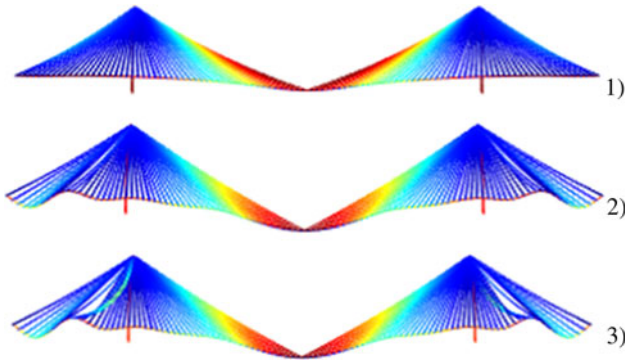

Fig. 12 Evolution of bridge deformed shape for the NLM model shown in Fig. 12a

Table 3 Influence of the parameters ε, a and p/g on the maximum load parameter λ_{max} for the nonlinear (NLM), linear (LM) and tension-only (TO) approaches for the discrete FE model

	a	0.10			0.20		
	ε	NLM	LM	TO	NLM	LM	TO
$p/g = 0.5$	0.2	7.848	5.305	5.305	7.731	4.320	4.314
	0.3	25.315	16.376	16.376	25.244	15.439	15.439
$p/g = 1$	0.2	5.589	3.838	3.838	5.544	3.146	3.140
	0.3	17.077	11.391	11.391	17.068	11.332	11.332

Uniform loading condition on the whole bridge length and H pylon shape

the pylon shape scarcely influences the non-linear static behavior of the bridge.

In general for the A pylon shape, involving larger lengths in the cable system, the bridge deformability increases and this causes a small reduction of the maximum load parameter λ_{max} with respect to the H pylon shape, that is confirmed by the numerical results.

Table 4 Influence of the parameters ε, a and p/g on the maximum load parameter λ_{max} for the nonlinear (NLM) and linear (LM) approaches for the discrete FE model

	a	0.10		0.20	
	ε	NLM	LM	NLM	LM
$p/g = 0.5$	0.2	2.393	3.021	2.188	2.599
	0.3	7.065	14.005	6.865	15.464
$p/g = 1$	0.2	1.673	2.237	1.557	1.950
	0.3	4.450	9.813	4.353	11.377

Central loading condition and A pylon shape

Table 5 Influence of the parameters ε, a and p/g on the maximum load parameter λ_{max} for the nonlinear (NLM) and linear (LM) approaches for the discrete FE model

	a	0.10		0.20	
	ε	NLM	LM	NLM	LM
$p/g = 0.5$	0.2	7.819	5.275	7.702	4.291
	0.3	25.188	16.274	25.115	15.338
$p/g = 1$	0.2	5.570	3.817	5.525	3.126
	0.3	16.994	11.322	17.020	11.180

Uniform loading condition on the whole bridge length and A pylon shape

4.3 Influence of load eccentricity and of pylon bending stiffness

In this section, for a given live to dead load ratio ($p/g = 1$), $a = 0.1$ and both $\varepsilon = 0.2$ (Fig. 14a) and 0.3 (Fig. 14b), the influence of the tower to girder bending stiffness ratio I_r on the maximum load parameter for loading in the central span and for the H pylon shape is analyzed, for different load eccentricity values e_c.

In Fig. 14a the plot of the maximum load parameter λ_{max} versus the tower to girder bending stiffness ratio I_r is presented for $\varepsilon = 0.2$. When I_r increases the maximum load parameter increases since the prebuckling configuration involves smaller deflections and the associated prebuckling behavior can be considered as linear owing to a negligible imperfection sensitiveness. On the other hand the effect of load eccentricity is appreciable only for $I_r < 5$, for which increasing load eccentricity leads to a transition from an in plane buckling to an out of plane buckling coupling pylons and girder. This behavior is related to different axial compressions in the two different towers of the pylon and to the different behavior of left and right stay systems with respect to pylon vertical axis, related to both the torsional rotation and nonlinear cable behavior, inducing a horizontal flexural couple acting as an imperfection in the activation of out of plane buckling. For $I_r > 5$ the effect of eccentricity is lower than 1 %.

For $\varepsilon = 0.3$, a similar trend (Fig. 14b) is obtained for the load maximum parameter but with a stronger influence of I_r, leading to an increase of 45 % up to $I_r = 70$, with the effect of eccentricity appreciable for a tower stiffness ratio $I_r < 1$ leading to local pylon buckling.

The influence of the tower to girder stiffness ratio, in the case of uniform loading condition on the whole bridge length and for the H pylon shape is represented in Fig. 15a and b, for $\varepsilon = 0.2$ and 0.3 respectively. In particular, for uniform load applied on the entire bridge deck the load maximum level is more than three times respect to central load. The effect of load eccentricity is larger respect to the central loading case, whereas also in this case pylon buckling occurs for small values of I_r.

A larger influence of the relative tower stiffness is evidenced for $\varepsilon = 0.3$ leading to a maximum increase of 16 % up to $I_r = 70$.

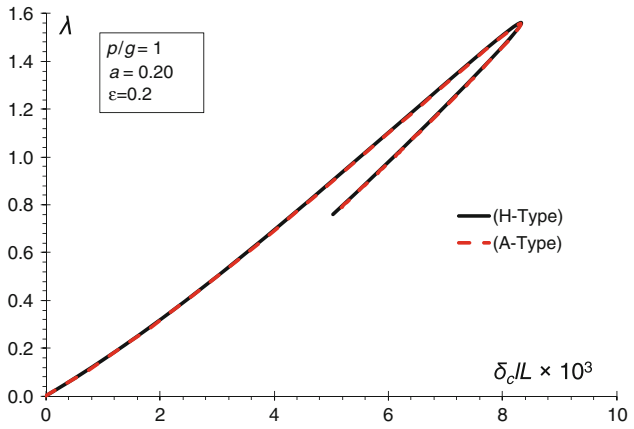

Fig. 13 Plots of the load parameter λ versus δ_c (central midspan deflection) for the central loading condition and $\varepsilon = 0.2$: H-type and A-type pylon shape

5 Conclusions

In this work a numerical investigation on the geometrically nonlinear static behavior of self-anchored long span cable-stayed bridges with a fan-shaped arrangement of stays is

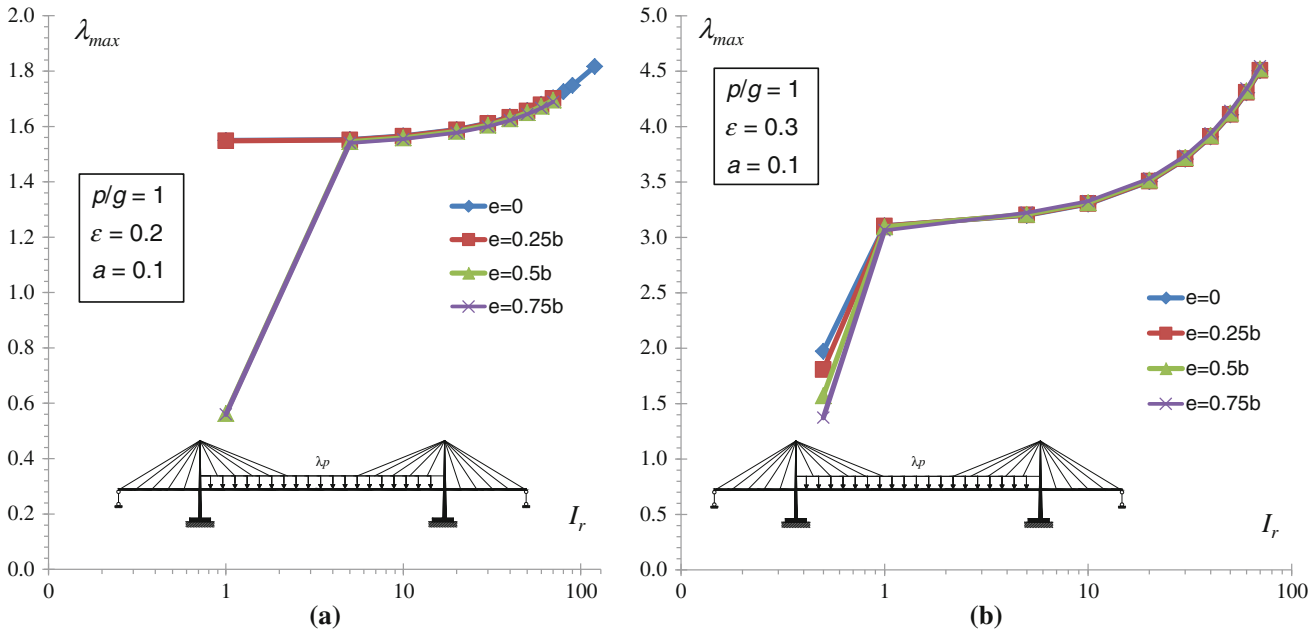

Fig. 14 Effect of pylon bending stiffness and of load eccentricity on the maximum load parameter (a = 0.1) for the central loading condition and H pylon shape: $\varepsilon = 0.2$ (**a**) and $\varepsilon = 0.3$ (**b**)

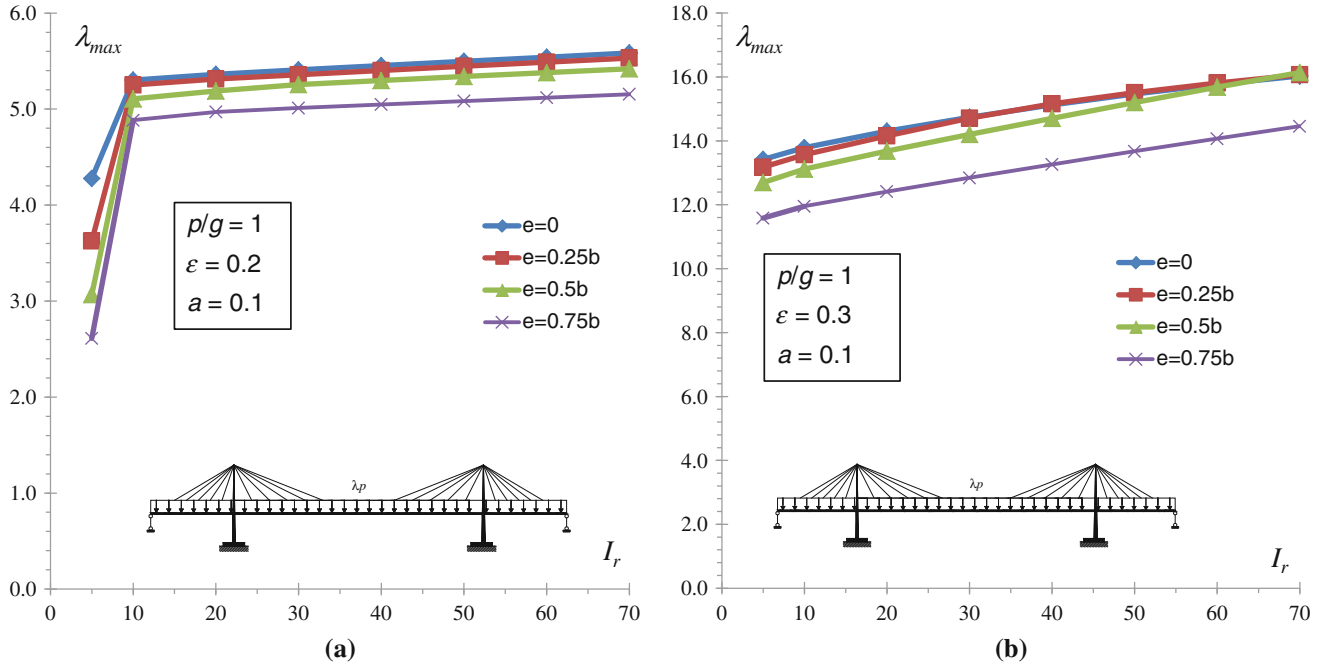

Fig. 15 Effect of pylon bending stiffness and of load eccentricity on the maximum load parameter (a = 0.1) for the uniform loading condition on the whole bridge length and H pylon shape: ε = 0.2 (**a**) and ε = 0.3 (**b**)

carried out by adopting a spatial finite element model of the bridge. Numerical computations are devoted to investigate the influence of three different stays response approaches on the bridge nonlinear behavior by using the more general 3D discrete model and adopting both the H and A pylon shapes. In particular, the mechanical response of a single stay has been modeled by using the multiple truss element nonlinear formulation (denoted as NLM), the tangent modulus linear model (denoted as LM) with the initial stress derived from the initial shape analysis and the tension only approximation (denoted as TO) according to which cable assumes a vanishing stiffness under shortening. The above analysis of the influence of different cable modeling techniques on nonlinear bridge behavior represents the main original contribution of the paper since this aspect has been scarcely analyzed in previous studies despite its significance for an accurate prediction of the bridge maximum load carrying capacity.

An equivalent continuous model of the bridge is also developed in order to point out the main parameters governing the non-linear behavior of the bridge to be used in the more general 3D discrete bridge model. Consequently, original parametric analyses are carried out to analyze the influence of the three stays response models on the nonlinear static behavior of cable stayed bridges, for different values of the relative bending stiffness ε, the live to dead load ratio p/g and the stay deformability parameter a, and for both the case of central loading and uniform loading on the whole bridge length.

Numerical results show the typical snapping behavior for high values of the load parameter λ due to the coupling between the instabilizing effect of the axial compression in the girder and the softening behavior of stays response in the lateral span, occurring in the case of the central loading condition. In particular, for this loading condition the load displacement diagrams exhibit a notable overestimation, in terms of the load parameter, for the LM approach whereas an underestimation for the TO one with respect to the actual behavior (NLM). Moreover, the numerical computations show the strong stabilizing effect of the girder stiffness independently on the adopted model.

In the case of the uniform loading on the whole bridge length, the nonlinear behavior is governed by the instabilizing effect of axial compression, while cables provide a stiffening effect except for a very small group of cables in the lateral span near the maximum load. Contrarily to the central loading condition, as the load parameter increases the effect of softening in stays tangent stiffness is negligible occurring for a very small group of cables and for larger load level, and the stays are characterized by tensile axial strains except near the load maximum. For this loading condition it is possible to appreciate the conservative behavior of the LM and TO models with respect to the NLM, in terms of the maximum load parameter λ_{max}.

Additional numerical results, obtained considering the A pylon shape for the bridge, are in agreement with those obtained for the H pylon shape and point out that in the case of the A pylon shape the bridge deformability

increases, causing a small reduction of the maximum load parameter λ_{max} with respect to the H pylon shape. Finally, a parametric analysis has been carried out in terms of live load eccentricity and pylon bending stiffness pointing out that the live load eccentricity effects are appreciable only for low values of the tower to girder bending stiffness ratio I_r, when a transition from in plane buckling to an out of plane buckling coupling pylons and girder may arise. The effects of load eccentricity are more appreciable in the case of the uniform loading case.

The above described parametric analyses represents another aspect of novelty of the paper since previous parametric studies available in the literature are characterized by various simplified assumptions and include only one or more sources of geometrically nonlinearities. For instance pylon nonlinearities have been often neglected, the analysis has been normally carried out excluding out-of-plane deformations, a linear prebuckling behavior has been frequently assumed, cable behavior has been usually simulated by using a single straight truss element incorporating sag effects by using the Dischinger tangent modulus often with a tension only behavior and the initial bridge configuration under dead loads has been typically determined by means of simplified techniques based on equilibrium requirements.

The results presented in the paper point out the central role of an accurate description of geometrically nonlinear effects arising from the stays nonlinear response in coupling with the instability effect of axial compression in girder and pylons, for an actual prediction of the nonlinear bridge behavior. These results evidence how the nonlinear stays response plays a strong role, especially when the assumed loading condition produces cable unloading, in coupling with the notable influence of the relative girder stiffness on the stability bridge behavior. On the other hand, generally speaking pylon shape and stiffness, live load eccentricity and torsional stiffness are less important factors in non-linear analysis.

References

1. Gimsing NJ (1983) Cable supported bridges: concepts and design. Wiley, New York
2. Leonhardt F Zellner W (1991) Past, present and future of cable-stayed bridges. In: Proceedings of the seminar of cable-stayed bridges. Recent developments and their future. Yokohama, Japan, 10–11 December, pp 1–33
3. Troitsky MS (1977) Cable-stayed bridge-theory and design. Crosby Lockwood Staples, London
4. Podolny WJ, Scalzi JB (1976) Construction and design of cable stayed bridge. Wiley, New York
5. Wang PH, Yang CG (1996) Parametric studies on cable-stayed bridges. Comput Struct 60(2):243–260
6. Wang P-H, Lin H-T, Tang T-Y (2002) Study on nonlinear analysis of a highly redundant cable-stayed bridge. Comput Struct 80:165–182
7. Tang CC, Shu HS, Wang YC (2001) Stability analysis of steel cable-stayed bridges. Struct Eng Mech 11:35–48
8. Adeli H, Zhang J (1995) Fully nonlinear analysis of composite girder cable-stayed bridges. Comput Struct 54(2):267–277
9. Song W-K, Kim S-E (2007) Analysis of the overall collapse mechanism of cable-stayed bridges with different cable layouts. Eng Struct 29:2133–2142
10. Seif SP, Dilger WH (1990) Nonlinear analysis and collapse load of P/C cable stayed bridges. J Struct Eng ASCE 116(3):829–849
11. Yoo H, Choi D-H (2009) Improved system buckling analysis of effective lengths of girder and tower members in steel cable-stayed bridges. Comput Struct 87:847–860
12. Bruno D, Grimaldi A (1985) Nonlinear behavior of long- span cable-stayed bridges. Meccanica 20:303–313
13. Freire AMS, Negrão JHO, Lopes AV (2006) Geometrical nonlinearities on the static analysis of highly flexible steel cable-stayed bridges. Comput Struct 84:2128–2140
14. Wang P-H, Tang T-Y, Zheng H-N (2004) Analysis of cable-stayed bridges during construction by cantilever methods. Comput Struct 82:329–346
15. Fleming JF (1979) Nonlinear static analysis of cable-stayed bridge structures. Comput Struct 10(4):621–635
16. Wang YC (1999) Number of cable effects on buckling analysis of cable-stayed bridges. J Bridge Eng 4(4):242–248
17. Ying X, Kuang JS (1999) Ultimate load capacity of cable-stayed bridges. J Bridge Eng 4(1):14–22
18. Janjic D, Pircher M, Pircher H (2003) Optimization of cable tensioning in cable-stayed bridges. J Bridge Eng ASCE 8(3): 131–137
19. Wang P-H, Tang T-Y, Zheng H-N (2004) Analysis of cable-stayed bridges during construction by cantilever methods. Comput Struct 82:329–346
20. Choi DH, Yoo H, Shin JI, Park SI, Nogami K (2007) Ultimate behavior and ultimate load capacity of steel cable-stayed bridges. Struct Eng Mech 27(4):477–499
21. Ernst HJ (1965) Der E-Modul von Seilen unter Beruecksichtigung des Durchhanges. Der Bauingenieur 40:52–55
22. Thai H-T, Kim S-E (2011) Nonlinear static and dynamic analysis of cable structures. Finite Elem Anal Des 47:237–246
23. Budiansky B (1974) Theory of buckling and post-buckling behavior of elastic structures. Adv Appl Mech 14:1–67
24. Bazant ZP, Cedolin L (1991) Stability of structures, elastic, inelastic, fracture, and damage theories. Oxford University Press, New York
25. Bruno D, Greco F, Lonetti P (2008) Dynamic impact analysis of cable-stayed bridges under moving loads. Eng Struct 30(4): 1160–1177
26. Bruno D, Leonardi A (1986) Non linear analysis of cable-stayed bridges eccentrically loaded. IABSE Periodica 4/1986 Proceedings P-103/86 10:129–140
27. Bruno D, Greco F, Lonetti P (2009) A parametric study on the dynamic behavior of combined cable-stayed and suspension bridges under moving loads. Int J Comput Methods Eng Sci Mech 10(4):243–258
28. Greco F, Lonetti P, Pascuzzo P (2013) Dynamic behavior of cable-stayed bridges affected by accidental failure mechanisms under moving loads. Mathematical Problems in Engineering, Volume 2013, Article ID 302706, 20 pp
29. Como M, Grimaldi A, Maceri F (1985) Statical behaviour of long-span cable-stayed bridges. Int J Solids Struct 21(8):831–850
30. Bruno D, Colotti V (1994) Vibration analysis of cable-stayed bridges. Struct Eng Int 4(1):23–28

31. Bruno D, Leonardi A (1997) Natural periods of long-span cable-stayed bridges. J Bridge Eng 2(3):105–115
32. Vairo G (2010) A simple analytical approach to the aeroelastic stability problem of long-span cable-stayed bridges. Int J Comput Methods Eng Sci Mech 11:1–19
33. Comsol AB (2012) Structural mechanics module user's guide
34. Raid K (1999) Some modeling aspects in the nonlinear finite element analysis of cable supported bridges. Comput Struct 71:397–412
35. Vairo G (2008) A quasi-secant continuous model for the analysis of long-span cable-stayed bridges. Meccanica 43:237–250
36. Vairo G (2009) A closed-form refined model of the cables' nonlinear response in cable-stayed structures. Mech Adv Mater Struct 16:456–466
37. Vairo G (2010) A simple analytical approach to the aeroelastic stability problem of long-span cable-stayed bridges. Int J Comput Methods Eng Sci Mech 11:1–19
38. Kanok-Nukulchai W, Hong G (1993) Nonlinear modelling of cable-stayed bridges. J Constr Steel Res 26(2–3):249–266
39. Wang PH, Tseng TC, Yang CG (1993) Initial shape of cable-stayed bridges. Comput Struct 21(8):831–850